SUPPLEMENTARY MATERIAL FOR:

Schizophrenia is defined by cell-specific neuropathology and multiple neurodevelopmental mechanisms in patient-derived cerebral organoids

Michael Notaras[1], Aiman Lodhi[1], Friederike Dundar[2], Paul Collier[1], Nicole Sayles[1], Hagen Tilgner[1], David Greening[3,4,5], and Dilek Colak[1,6,*]

[1] Center for Neurogenetics, Feil Family Brain and Mind Research Institute, Weill Cornell Medical College, Cornell University, New York, New York, USA.
[2] Department of Physiology and Biophysics, Weill Cornell Medical College, Cornell University, New York, New York, USA.
[3] La Trobe Institute for Molecular Science, La Trobe University, Melbourne, Australia.
[4] Central Clinical School, Monash University, Melbourne, Australia.
[5] Baker Institute & Baker Department of Cardiometabolic Health, University of Melbourne, Melbourne, Australia.
[6] Gale and Ira Drukier Institute for Children's Health, Weill Cornell Medical College, Cornell University, New York, New York, USA.

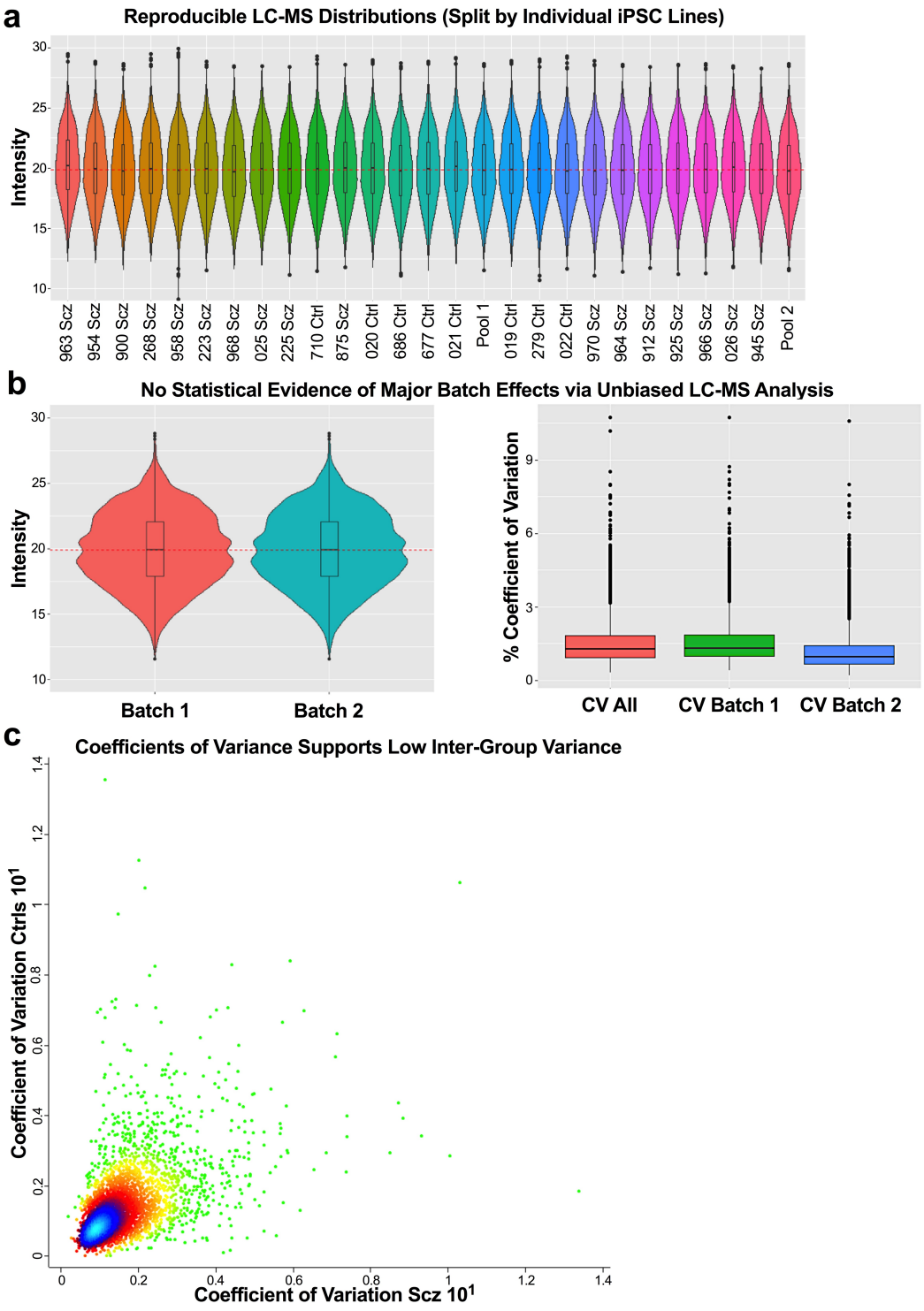

Figure S1. Establishing organoid reproducibility via computational analysis. To confirm the reproducibility of our cerebral organoid cultures within a larger cohort (*n* = 25 unique biological donors), we employed new analytical tandem-mass tag (TMT) chemistry that allowed multiplexing of 16 samples (16-plex) with high-resolution quantitative mass spectrometry. Because of our large cohort size and the need to include internal reference pools (see below), we generated

organoids from *n* = 25 lines in two distinct batches that could be tested for 1) batch effects, 2) inter-sample variance, and 3) overall reproducibility between individual iPSC donors within a given group. This allowed for a high-throughput and statistically unbiased evaluation of variation within our organoid cultures across lines and independently generated batches. For each TMT set (16-plex) we applied batch-specific normalization using global external pooled reference standards so that all *n* = 25 iPSC donors could be combined and examined together. Each 16-plex experiment contained a pooled reference label (134 isobaric label) that consisted of the same peptide digest from organoid lysates. Proteomic analysis of organoids from *n* = 25 iPSC lines (*n* = 8 Ctrl iPSC lines and *n* = 17 Scz iPSC lines) yielded 33,711 identified fragments and 3,910 quantifiable data points that could be used as an unbiased sample for computational analysis of organoid variance and reproducibility. No imputation of missing values was performed in any cohort, statistical *q* values were generated for each LC/MS data point, and all *p* values were corrected for multiple hypothesis testing.

a, Orthogonal LC/MS analysis split by iPSC line supports organoid reproducibility.

To provide an unbiased evaluation of LC/MS intensities, data distributions are provided for each individual iPSC line. Likewise, to evaluate coefficients of variance between all lines, we generated correlation matrices that revealed a high degree of similarity between all samples within two independent batches of organoids and iPSC donors. This confirms that organoids exhibited comparably low variance between individual iPSC donors.

b, Orthogonal LC/MS analysis revealed no major evidence of batch effects.

Between batches, there was a high degree of similarity in the LC/MS intensity maps and their density distributions. Critically, the generation of coefficients of variance for LC/MS data supported this interpretation. Namely, box-and-whisker plots revealed that coefficients of variation were less than 2% between batches (black bars denote median; boxes denote upper and lower quartiles; whiskers denote extremes). Analysis of individual batch variance consequently revealed variance of less than 2%. Together, these unbiased computational data confirm that there was no evidence of batch effects between organoids or within groups.

c, Orthogonal LC/MS analysis also confirms inter-group reproducibility.

Correlation analysis revealed that each batch following pooled reference normalization exhibited similar group variance. In sum, this analytical and unbiased approach to defining the variance within our cerebral organoid cultures is consistent with our ability to replicate and reproduce core phenotypes multiple times throughout our manuscript. This analysis therefore provided an unbiased, and computationally-derived, validation for baseline reproducibility of organoids between- and within-lines, which is consistent with prior analysis that cerebral organoids hold suitable construct-validity as a model of *in utero* human brain development [1-3].

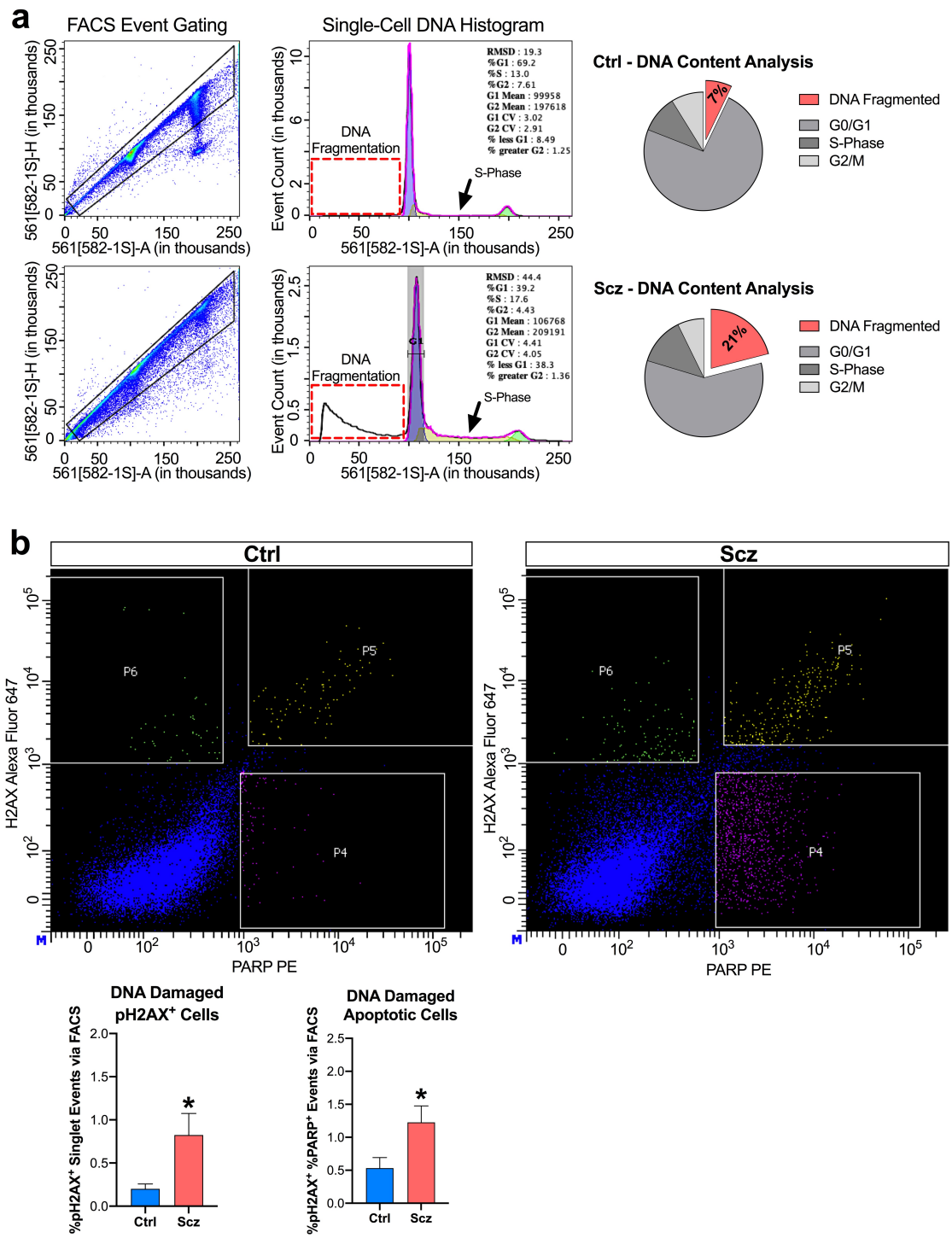

Figure S2. Validation of cell death in Scz organoids via DNA fragmentation, DNA damage induction, and single-cell PARP+ expression analysis.
In the main manuscript, we replicated an increase in progenitor cell death via colocalization with cleaved CAS3 (fig. 1, 4, and 5). However, we also sought to validate the increase in apoptosis via an unbiased, DNA-based, methodology to ensure that apoptosis induction in Scz organoids could be orthogonally validated.

a, Single-cell DNA content supports increased cell death in Scz organoids. To provide unbiased validation of increased apoptosis in Scz, we subjected a cross-sectional cohort of Ctrl and Scz organoids to a cellular DNA content analysis using Propidium Iodide (PI), flow cytometry, and FlowJo modeling. This allows live and dead cells to be detected based on their DNA content. Notably, when cells undergo apoptosis, DNA becomes fragmented. To reduce sample heterogeneity while promoting power, approximately 10 organoids were pooled per iPSC line (n = 9 total lines, 3 Ctrls and 6 Scz), dissociated into a single-cell suspension, and subjected to single-cell DNA content analysis via high-throughput flow cytometry. This analysis revealed that there was an approximately 3-fold increase in DNA fragmentation in Scz organoid samples (~7% in Ctrls vs ~21% in Scz organoids; see red dotted box in panel a). Additionally, Scz organoids also tended to exhibit a slightly elevated proportion of S-phase cells based on cellular DNA content (see black arrows in panel a). When coupled with an increase in DNA fragmentation, an alteration in S-phase may be indicative of a potential DNA-related mechanism that leads to cell cycle abortion and increased death of proliferating progenitors within Scz organoids.
b, Increased pH2AX recruitment is linked to cell death in Scz organoids. H2AX is involved in DNA damage [4] and DNA double-strand break repair [5], and is commonly induced during cellular division if DNA damage/breaks have occurred [6]. Phosphorylation of H2AX (pH2AX, gate p6) indicates the presence of DNA damage machinery [7], and if pH2AX is co-expressed with a cell death factor (e.g. cleaved PARP, gate p4) then DNA damaged dying cells are deemed to have been targeted for death (gate p5). Therefore, based on our neural progenitor cell death and single-cell DNA content analyses, we hypothesized that there would be an increased number of cells exhibiting pH2AX+ (p6) as well as pH2AX+ and PARP+ (p5) expression within Scz organoids. Organoids were sampled as described above from a pseudorandomly selected cross-section comprising n = 7 lines (3 Ctrls and 4 Scz). As expected, we detected an increased percentage of pH2AX+ and pH2AX+/cleaved PARP+ double-positive cells in Scz organoids. This data therefore provides yet further validation of increased cell death in Scz organoids, and suggests that cell death in Scz organoid is related to DNA damage.
Graphed data points reflect the average of iPSC lines.
*p < 0.05. Error bars reflect Standard Error of the Mean. Control, Scz: Schizophrenia.

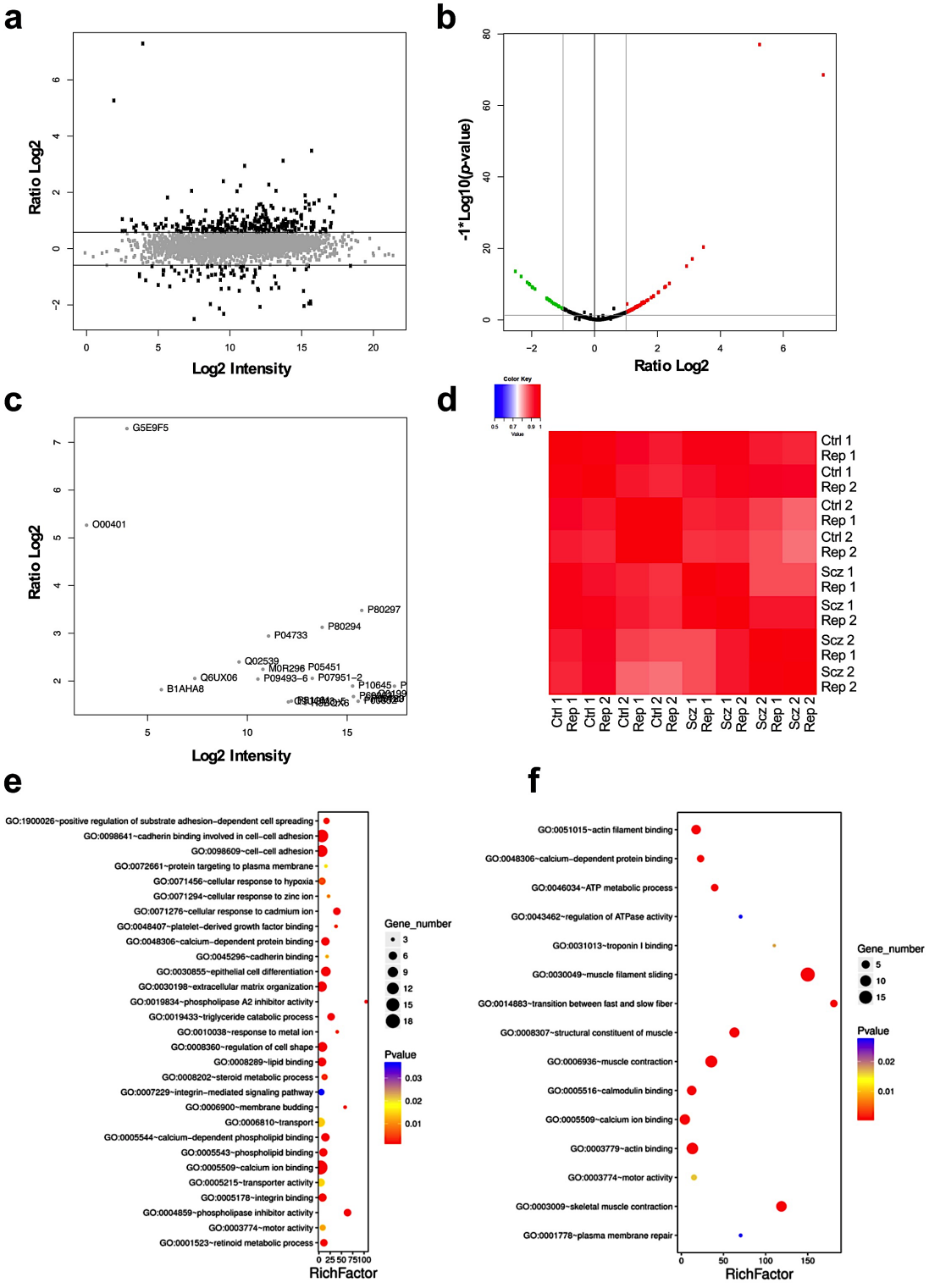

Figure S3. Further computational analysis of the Scz organoid proteome. a-c, WASL and MPV-17 are novel factors expressed in Scz organoids. Shown are ratio Log2 against Log2 intensity (a), a volcano plot parsing ratio Log2 by -1*Log10 (*p*-value) (b), and differentially expressed proteins mapped by protein identifiers (c). As can be seen across these panels, differential expression

within the Scz organoid proteome was limited to relatively few targets, suggesting specificity in those proteins that were significantly differentially expressed. The two proteins which with high ratio Log2 values relative to Log2 intensity were WASL (N-WASP) and MPV-17, which were the only two unique proteins detected in Scz organoids. Of note, transcripts for these factors were detected in Ctrl and Scz organoids in single-cell sequencing, but post-translational detection via TMT-LC/MS was restricted to Scz organoid samples. This suggests that N-WASP and MPV17 may be translationally repressed in Ctrl but not Scz organoids. While the functions of MPV17 to Scz remain unclear, the localization of this protein to mitochondria may be indicative of mitochondrial alterations in Scz organoids. Indeed, potential mitochondrial dysfunction in Scz postmortem brains has been reported [8], and mtDNA depletion has been reported in a family with psychosis [9]. Our other novel factor, N-WASP (*WASL*), has a role in cytoskeletal actin assembly that supports dendritic spines [10]. Dendritic spines are typically disrupted in pyramidal layer 3 cells in postmortem Scz tissue [11, 12], where expression of *WASL* also happens to be depleted in postmortem Scz tissue [13]. The post-translational expression of N-WASP (*WASL*) in Scz organoids therefore suggests that this molecule may play a role in early Scz neuropathology in the developing cerebral cortex.

d, High reproducibility of whole-organoid proteomes across groups. Shown is a heat map exhibiting all group and replicate samples, which exhibited both 1) global, 2) inter-group, and 3) inter-line reproducibility per coefficient of variance metrics. This once more provides validation of the high reproducibility and low variance of our experimental organoids. Individual protein variation across the proteome was similar across groups and is provided in Figure 2c.

e-f, Gene ontology and KEGG pathway analysis of the organoid proteome. Shown are up-regulated (e) and down-regulated (f) protein sets (f; defined as ±1.0 Log2, $p < 0.05$) in Scz patient-derived organoids. Y-axes represent gene ontology (biological process, molecular function, and pathway), and X-axes represents enrichment factor (rich factor = amount of differentially expressed proteins enriched/amount of all proteins in background gene set). Size and color of individual bubbles represents amount of differentially expressed proteins enriched in pathway and enrichment significance, respectively.

Ctrl: Control, Scz: Schizophrenia.

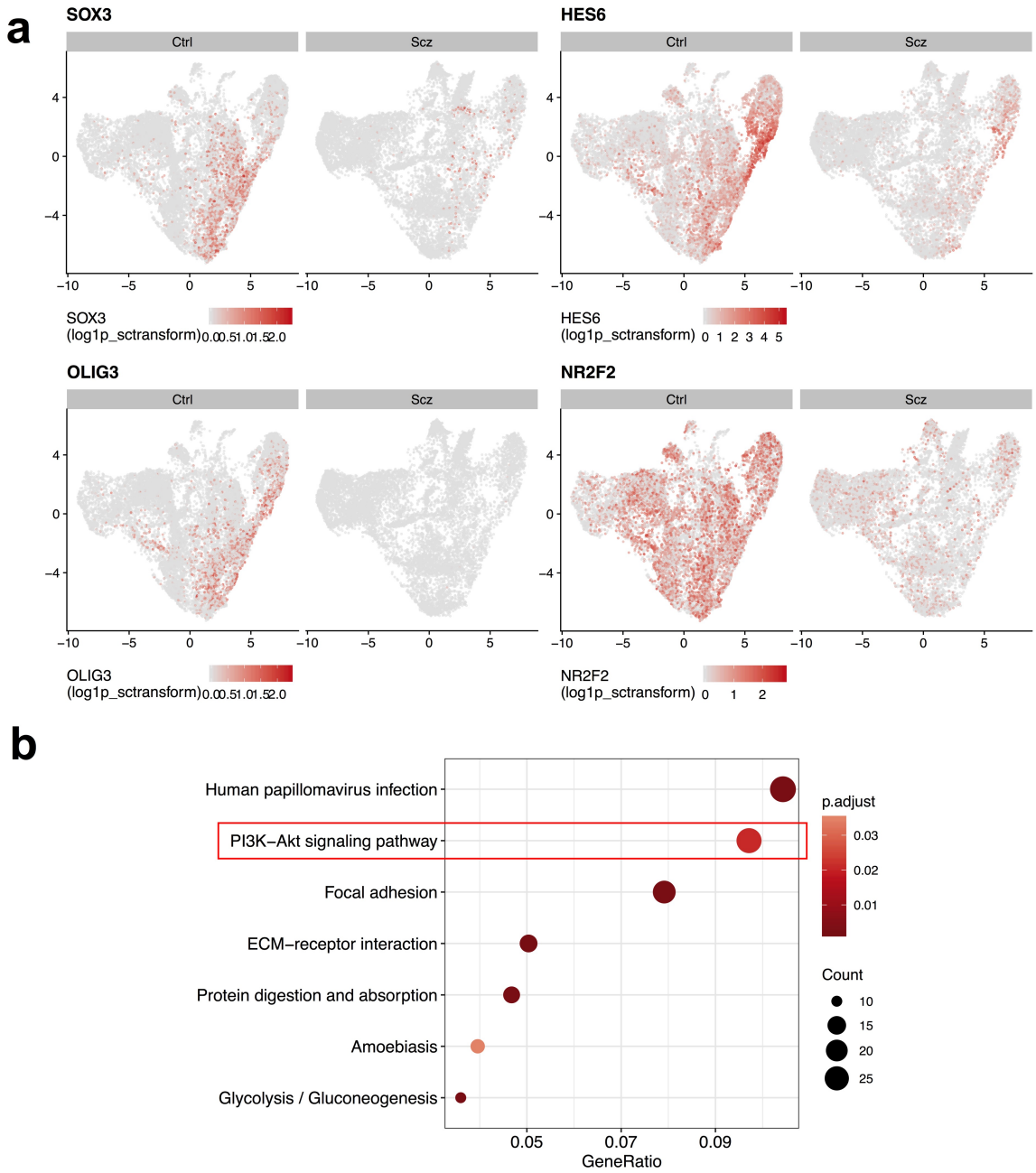

Figure S4. Further computational analysis of single-cell transcriptomes.
a, Down-regulated expression of developmental factors in Scz organoids. Shown are a selection of four noteworthy developmental factors found to be unbiasedly depleted in Scz organoids. Each of these factors has known roles in brain development and/or neuronal maturation. This is consistent with the remodeling of Scz progenitors away from neuron production (fig. 1-3).
b, Additional KEGG plot of pathway analyses of Scz neurons. Because only our GO pathway analysis of Scz neurons were not shown in fig. 3 for consistency sake, here we present the outcome of an alternative KEGG pathway analysis in neurons. Note enrichment for factors that belong to PI3K-Akt signaling (a primary neurotrophin/growth factor signaling cascade; see red box).

Note, enrichment does not necessarily depict up- or down-regulation, rather just factor-counts belonging to these biological processes (thus, individual factors in this enriched pathway may be differentially up- or down-regulated, indicating the potential for broader pathway dysfunction).
Ctrl: Control, Scz: Schizophrenia.

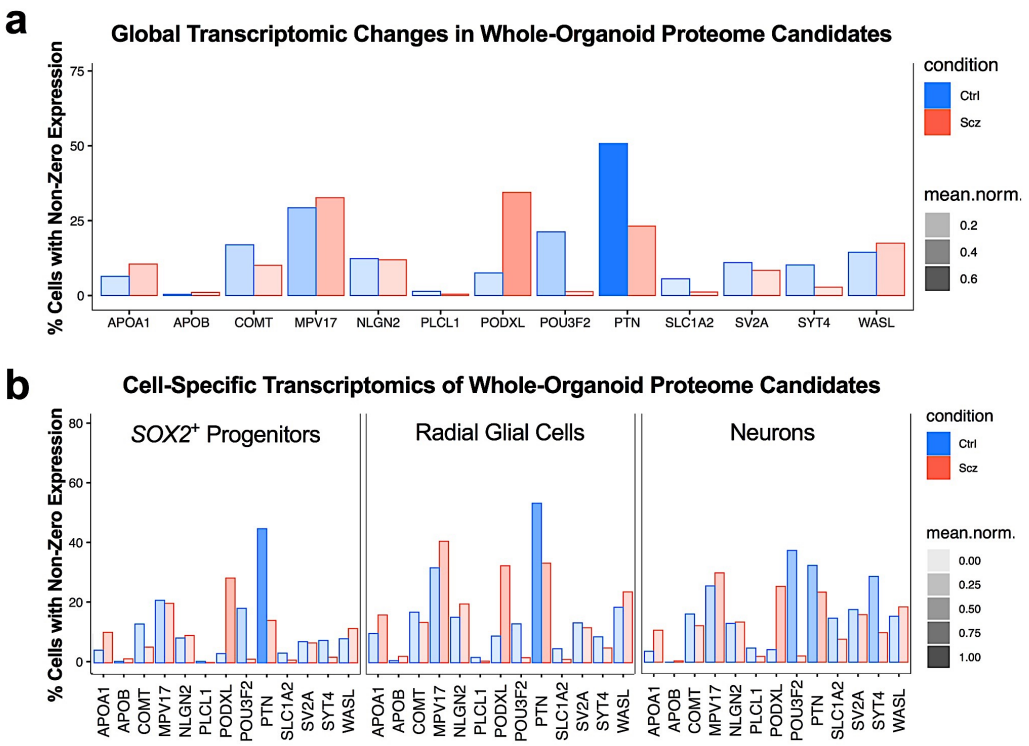

Figure S5. Cell-specific analysis of proteome targets in Scz organoids.
a, Global gene-expression of proteome targets in Ctrl and Scz organoids. Unbiased analysis of the Scz organoid proteome unveiled that Scz organoids principally differed from Ctrl organoids in the quantity of differentially expressed molecular factors (fig. 2e). This included novel targets that regulate development (e.g. POU-domain transcription factors, e.g. POU3F2/BRN2) or were implicated in genetic risk for Scz in large-scale GWAS and/or meta-analysis (e.g. PTN, PLCL1, COMT, and PODXL, see main text). We cross-referenced expression of these factors in a global analysis of single-cell transcriptomes and found that gene-expression of the forebrain-specific neuronal transcription factor *POU3F2* (BRN2) was down-regulated. Similarly, gene expression of Scz risk candidates *PTN*, *COMT*, and to a lesser extent, *PLCL1*, were also down-regulated. Consistent with proteomics, expression of *PODXL* remained up-regulated in global analysis of Scz transcriptomes.
b, Cell-specific analysis of proteome targets reveals nuanced expression. Next, we sought to resolve cell-specific contributions to expression differences as well as gene-expression levels in Scz progenitors and neurons. Thus, we analyzed our scRNA-Seq dataset by cell type (fig. 3h-l and S4). This analysis revealed a striking depletion of *POU3F2* (BRN2) and PTN in Scz progenitor cell-types, as well as a reduction in Scz neurons (as shown in fig. 3). Similarly, *COMT* appeared to be more prominently altered in Scz progenitors, relative to Scz neurons. *PLCL1* expression was more prominently reduced in Scz neurons relative to Scz progenitors. *PODXL* gene-expression was up-regulated in both progenitors and neurons. Ctrl: Control, Scz: Schizophrenia.

a

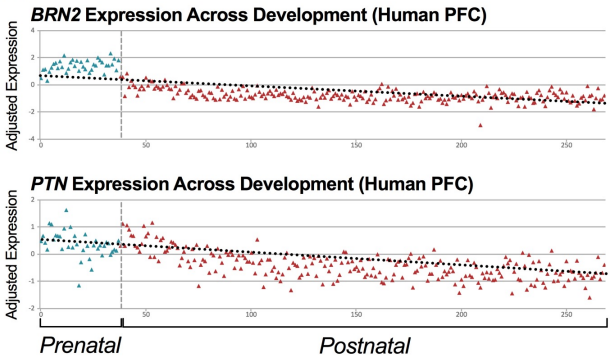

n = 269 time-points, including *n* = 38 human fetal samples.

b

SZDB and SZGR Database Hits of Scz Genome-Wide Association

Gene	Loci	Index SNP	*p*-value	Loci	Meta-Analysis	Hit	GWAS & Size
BRN2	-	-	-	-	-	-	-
PTN	7:137039644-137028611	rs3735025	7.02e-11	55	✔	✔	CLOZUK *n* = 35,802
PTN	7:137039644-137028611	rs3735025	3.28e-09	62	✘	✔	PGC *n* = 150,064

c

SZDB and SZGR Differential Methylation Database Hits

Gene	Tissue	*Probe Location*	*p*-value	Corrected Value	Study & Size
BRN2	Prefrontal Cortex	6:99280108	7.81e-09	3.57e-03	Jaffe et al. *n* = 108 Scz *n* = *136* Ctrls
BRN2	Blood	6:99282348	3.34e-02	-	Kinoshita et al. *n* = 63 Scz *n* = 42 Ctrl
PTN	Prefrontal Cortex	7:136989898	1.21e-05	1.35e-02	Wockner et al. *n* = 24 Scz *n* = 24 Ctrls

Figure S6. Orthogonal validation of BRN2 and PTN disease relevance via informatic mining of human Scz studies and Scz database repositories. To provide further insight into the disease relevance of our candidate rescue factors, PTN and BRN2, we consulted large-scale data repositories that have indexed, pooled, or compiled the results of human brain tissue arrays, GWAS, and other commonly employed techniques in Scz association studies.
a, *BRN2* and *PTN* are enriched during prenatal human cortex development. To orthogonally validate BRN2 and PTN as embryonic active factors in the developing cortex of humans, we mined the BrainCloud™ (dbGaP Accession: phs000417.v2.p1; [14]) dataset that has quantified gene expression in the human brain across the lifespan. This yielded data congruent with enrichment patterns observed in our organoid cultures, whereby *BRN2* (ProbeID: hHR008743, EntrezID: 5454) and *PTN* (ProbeID: hHC023376, EntrezID: 5764) were expressed in the embryonic human PFC. Additionally, relative to expression patterns across the lifespan, BRN2 and PTN are also enriched during human

prenatal development (*n* = 269 human sample time points, including *n* = 38 human fetal samples; dotted lines reflect an approximate line of best fit). These data thus provide orthogonal validation that PTN and BRN2 are transcriptionally enriched during embryonic development of the human cortex.

b-c, An index SNP in proximity to *PTN* exhibits gene association in Scz. As discussed in the main manuscript, PTN has been associated with Scz. Here we sought to explore this relationship further by leveraging the Schizophrenia Database (SZDB) [15] and Schizophrenia Gene Resource (SZGR) v2.0 [16, 17]. Both of these references function as multi-omics data repositories that aggregate data from genetic, transcriptome, and epigenetic Scz association studies. Searching these databases and datasets yielded several positive associations of PTN and BRN2 to Scz. This included an index SNP (rs3735025) in proximity to PTN that exhibited genome-wide association within two of the largest Scz cohorts ever studied (total *n* = 35,802 [18] and *n* = 150,064 [19] humans, respectively; see tabulation in b). Additionally, analysis also revealed positive association of both BRN2 and PTN in differential methylation of samples from Scz patients (see [20-22] and tabulation in c for dataset summary). When combined, these data provide orthogonal validation that both of our candidate targets maintain disease relevance to Scz in human association studies.

PFC: Prefrontal cortex.

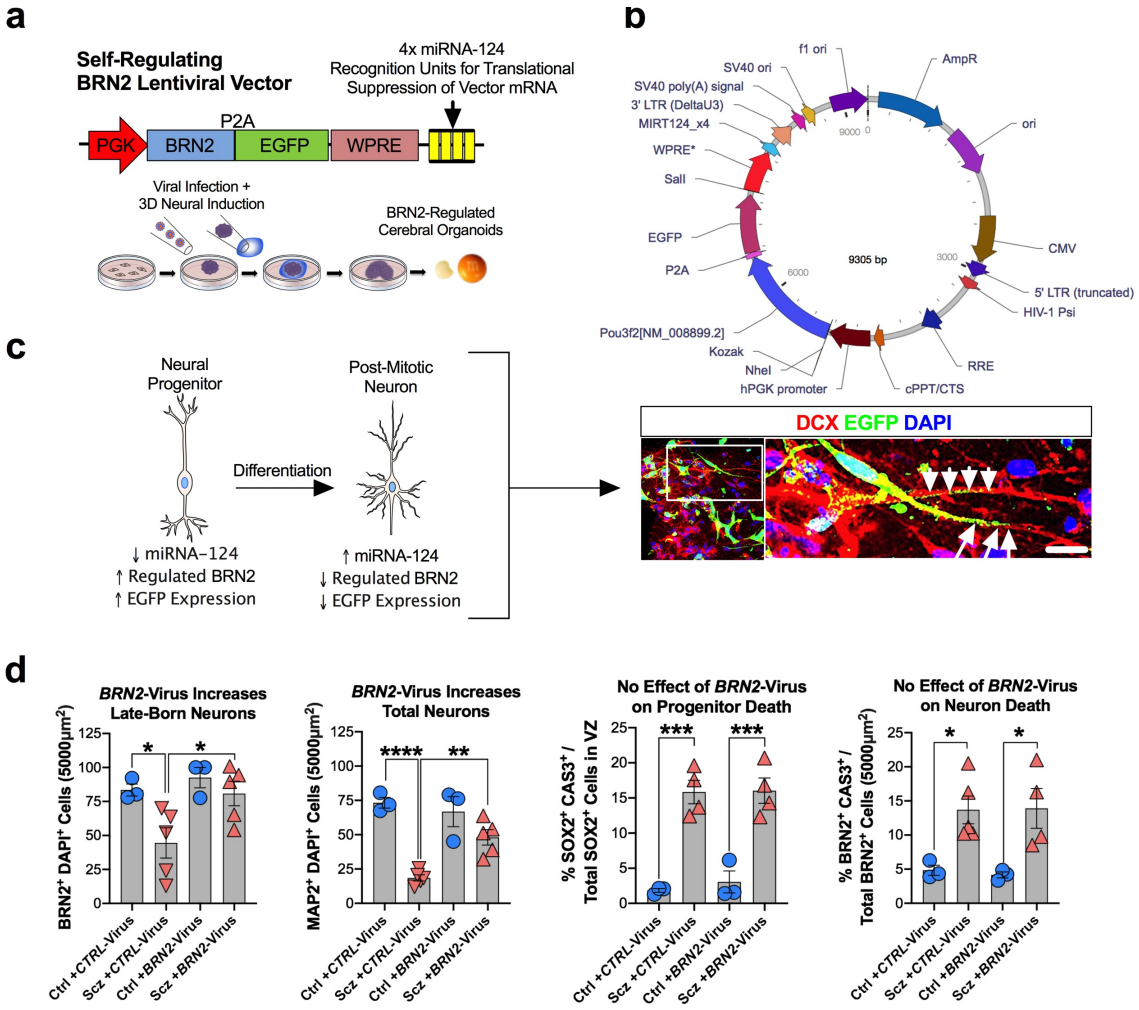

Figure S7. Supplementary information for BRN2 rescue experiments in Scz patient-derived organoids.

a-c, Design of *BRN2*-Virus for rescue experiment in Figure 5.

Our *BRN2*-Virus is a self-regulating construct designed to be translational suppressed when infected cell-types differentiate into post-mitotic neurons. Thus, sustained overexpression can be induced transiently without continuing to influence neurons. This allowed us to determine in figure 4 that BRN2 influences neuronal differentiation but not survival in Scz organoids. The *BRN2*-Virus construct was adapted from a previously validated construct, but was modified to contain an EGFP reporter construct for visualization (see technical details in Materials and Methods). Our simplified experimental timeline (a) from Figure 5 is provided along with viral construct (b) for comparison and additional details not included in main text for both brevity and simplicity. Also shown is a high-magnification image from within a 3D organoid infected with *BRN2*-Virus that visualizes self-regulated translational suppression via loss of EGFP signal in a differentiating progenitor (arrows) and a new-born neuron (arrowheads; c). As expected, *BRN2*-Virus expression was only observed in progenitors and differentiating cells, but not in mature postmitotic neurons.

d, Confirmation that *BRN2*-Virus regulates neuron numbers in Scz organoids when data are analyzed by the average of iPSC lines.
For transparency, here we provide an alternative visualization of *BRN2*-Virus rescue data whereby raw data have been collapsed into the average of iPSC line (each data point here reflects the average of quantifications from an iPSC line). As can be seen in the leftmost panels, *BRN2*-Virus significantly increased neuron numbers when two independent neuronal antigens (BRN2 and MAP2) were utilized for immunohistochemistry and neuron quantifications. Consistent with the data shown in figure 4, neither progenitor nor neuronal survival were rescued by *BRN2*-Virus Scz organoids when the average of iPSC lines was analyzed. Thus, as discussed in the main text, BRN2 was shown to regulate neuron numbers but not cell death phenotypes in Scz organoids.
*$p < 0.05$, **$p < 0.01$, ***$p < 0.001$, ****$p < 0.0001$. Scale: c = 20μm. Error bars reflect Standard Error of the Mean. Ctrl: Control, Scz: Schizophrenia, EGFP = Enhanced green-fluorescent protein.

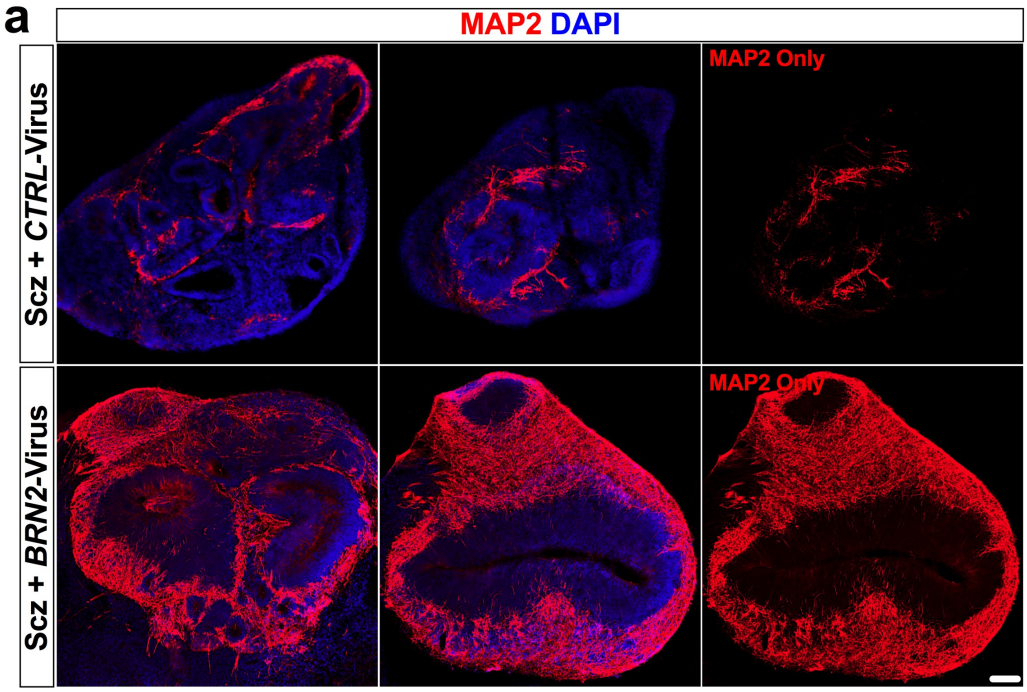

Figure S8. Enlarged whole-organoid images of *BRN2*-Virus modulation of neuron numbers within Scz organoids.
To provide additional visualization, we sought to provide additional whole-organoid images of the *BRN2*-Virus rescue effects on neuron numbers in Scz organoids. In the main figures, individual fields were quantified and shown which are representative of both sampling and reported phenotypes. Here we provide whole-organoid images to complement these visualizations, and to exemplify the extent of rescue achieved at the whole-organoid level. Two independent organoids are shown for each treatment group for confirmation of phenotype reproducibility. Note, MAP2 has been presented as an isolated channel for one organoid set for clarity and transparency so that the extent of MAP2 depletion can be observed at baseline in Scz organoids that received *Ctrl*-Virus and the extent of rescue achieved in Scz organoids following infection with *BRN2*-Virus. Note that multiple independent organoids have been selected in the manuscript here to provide numerous independent visualizations of core phenotypes and their rescue in Scz organoids. Scale bar: 60μm.

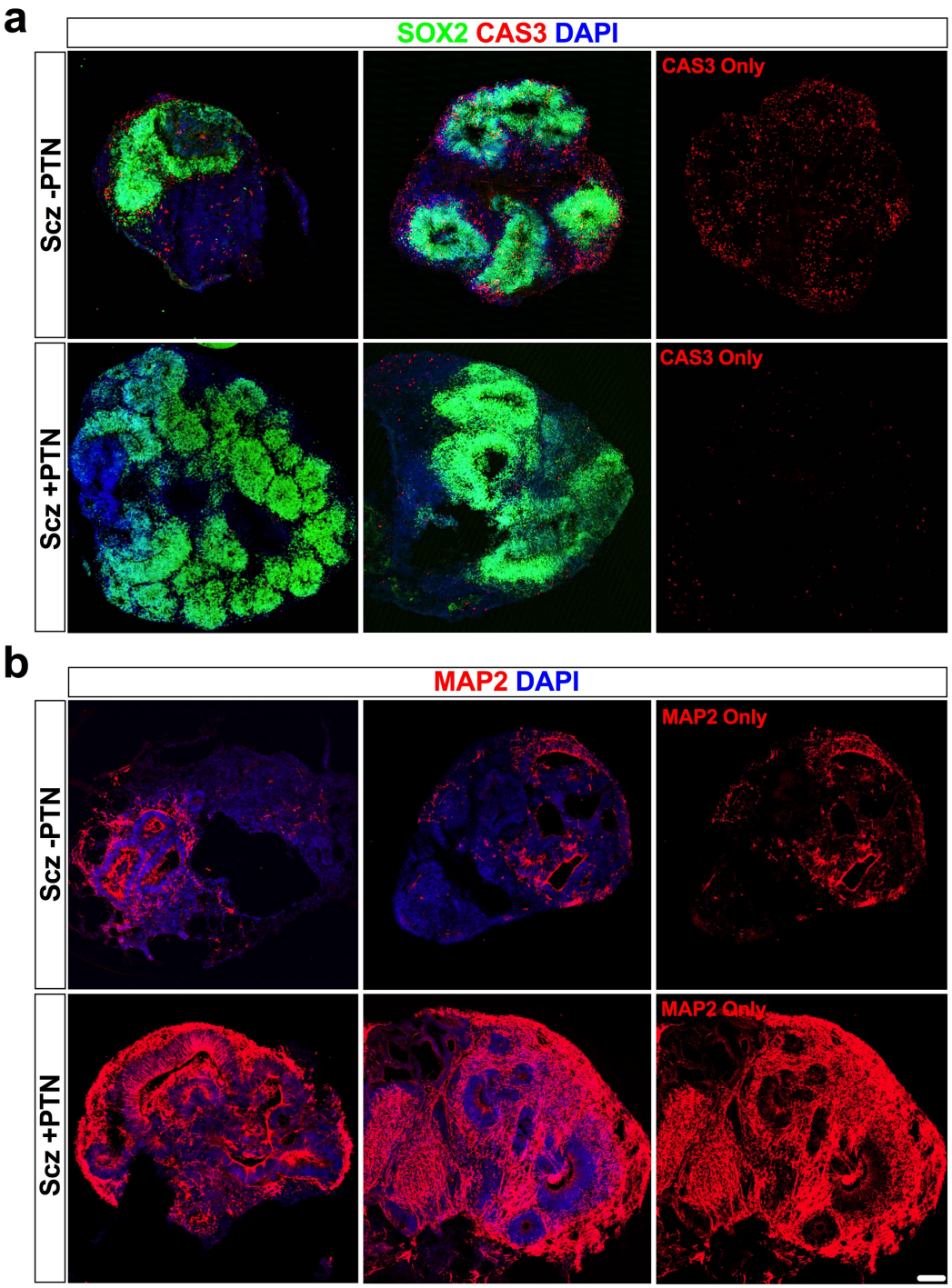

Figure S9. Whole-organoid images of PTN rescue effects in Scz samples. To provide additional visualization, we sought to provide additional whole-organoid images of PTN rescue effects in Scz organoids. In the main figures, individual fields were quantified and shown which was representative of both sampling and reported phenotypes. Here we provide whole-organoid images to complement these visualizations, and to exemplify the extent of rescue achieved at the whole-organoid level.

a, Whole-organoid visualization of progenitor cell death in Scz organoids at baseline and following PTN treatment.
Two independent organoids are shown for each treatment group for confirmation of phenotype reproducibility. Note, cleaved CAS3 has been presented as an isolated channel for one organoid set for additional transparency.
b, Whole-organoid visualization of neurons in Scz organoids at baseline and following PTN treatment.
Once more, two independent organoids are shown for each treatment group for confirmation of phenotype reproducibility. MAP2 has been presented as a split channel for one organoid set for transparency. Note that multiple independent organoids, and fields within them, were shown across the manuscript to provide numerous independent visualizations of core phenotypes and their rescue in Scz organoids. Scale bar: 60 μm

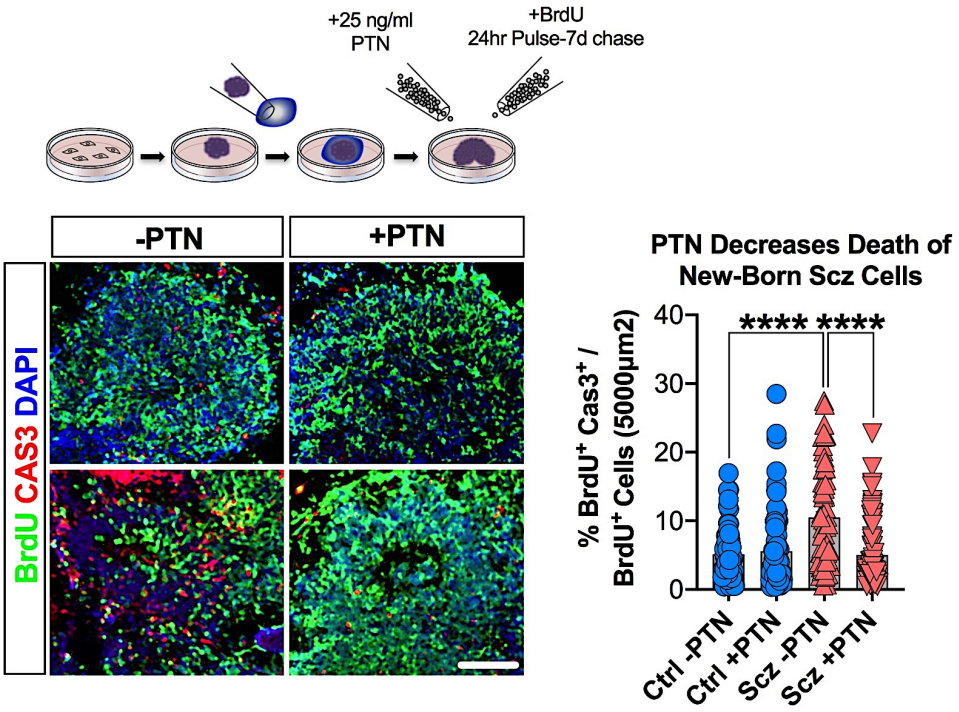

Figure S10. PTN improves new-born cell survival in Scz organoids.
In figure 5, we show that PTN-supplemented Scz organoids exhibited increased progenitor survival and neuronal differentiation. In addition to these phenotypes, we also assessed the overall survival of new-born cells labeled with BrdU as per our pulse-chase paradigm (see fig. 1 and 5, as well as our schematic above). PTN-supplemented Scz organoids exhibited significantly decreased new-born cellular death (Vehicle Ctrl *n* = 71 fields, *n* = 24 organoids, from *n* = 4 independent Ctrl iPSC lines, PTN-Supplemented Ctrl *n* = 95 fields, *n* = 30 organoids, from *n* = 4 independent Ctrl iPSC lines; Vehicle Scz *n* = 69 fields, *n* = 24 organoids, *n* = 4 independent Scz iPSC lines, PTN-Supplemented Scz *n* = 89 fields, *n* = 26 organoids, from *n* = 4 independent Scz iPSC lines). All graphed data represent unique, non-overlapping, fields. Together with data in fig. 5, these data indicate that in Scz organoids PTN exerts putative neurotrophic-like effects by promoting cellular survival. Thus, in Scz organoids, reconstitution of PTN as an exogenous morphogen facilitated progenitor survival and neurogenesis that resulted in the rescue of neuron numbers in Scz cortical fields.
****$p < 0.0001$. Scale: 60µm, Error bars reflect Standard Error of the Mean. Ctrl: Control, Scz: Schizophrenia.

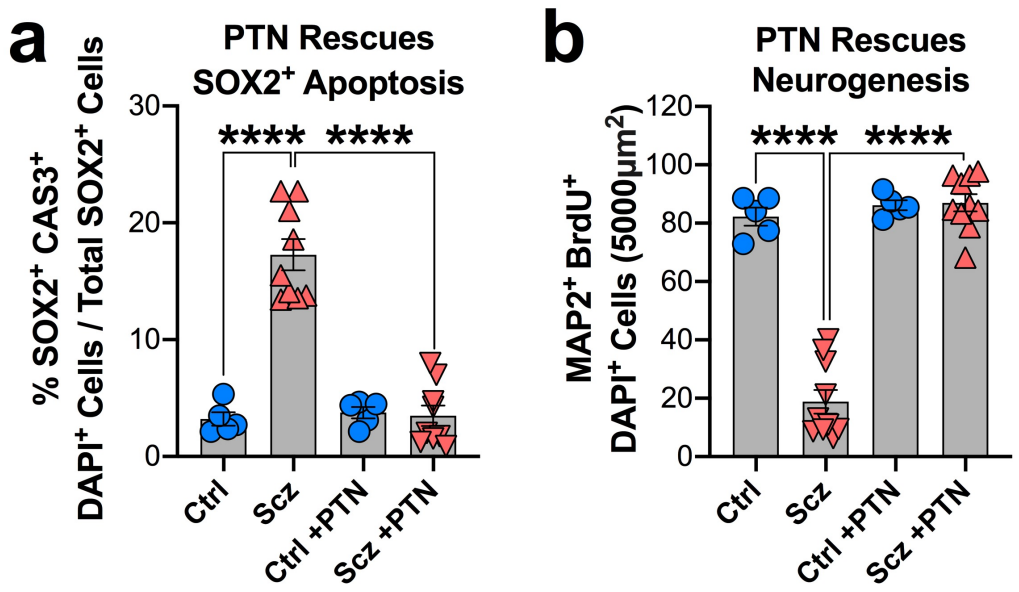

Figure S11. Analysis of PTN rescue phenotypes by the average of iPSC lines within groups, including graphing of raw data split by iPSC line. For transparency, visualization of Scz core phenotypes (both at baseline and following PTN treatment) have been provided here as an average of lines. This allows the relative consistency of Scz phenotypes to be assessed by the average of each patient iPSC line both with and without PTN treatment. As can be seen, phenotypes were broadly reproducible across individual lines, and all patient lines included in the PTN rescue experiment exhibited consistency in phenotype via restoration and/or improvement following PTN treatment.

a, Donor-split analysis of progenitor death in Scz organoids. Analysis of progenitor death confirmed that Scz organoids exhibited increased SOX2+ cell death in ventricular zones, and that PTN treatment could negatively regulate SOX2+ cell death in Scz organoids. In the iPSC donor-split analysis, each data point represents the average of each single iPSC donor. Final ventricular zone analysis numbers are provided in the figure legend of the manuscript (fig. 5), with this analysis reflecting *n* = 5 Ctrl and *n* = 9 Scz iPSC donors (total *n* = 14 iPSC lines).

b, Donor-split analysis of neuronal depletion and death in Scz organoids. Analysis of neuronal depletion via quantifications of MAP2+ BrdU+ cells revealed that PTN treatment positively regulated neuron numbers. In the iPSC donor-split analysis, each data point represents the average of each single iPSC donor. field. Final field analysis numbers are provided in the figure legend of the manuscript (fig. 5), with this analysis reflecting *n* = 5 Ctrl and *n* = 10 Scz iPSC donors (total *n* = 15 iPSC lines). For consistency, data are provided in the same format as our BRN2 rescue experiment (see donor-split analysis in fig. S7).

Supplementary Table 1. Clinical notes of NIMH-deposited Scz iPSC lines.

NIH iPSC Scz Line	Sex	Ethnicity	Age of Sampling	Age of Onset	Clinical Notes
MH0159025	Male	White	48	41	Paranoid Scz. Cannabis & alcohol abuse, drug overdose history, father had depression/drug abuse history, one sibling has bipolar disorder, behavioral problems from age 10.
MH0159026	Male	White	60	38	Persistent auditory hallucinations, lifetime cannabis & alcohol abuse, nicotine addiction, brother had schizophrenia.
MH0185223	Male	White	26	-	Episodes of agitation, delusions of persecution, and fear of assassination; at age four mild features of pervasive developmental disorder, Scz/SA/ASD father and sister, brother autistic at age four
MH0185225	Male	White	23	-	Paralogical thinking, affective shielding, splitting of affect from content, suspiciousness, SZ/SPD father, anorexic/schizoid sister.
MH0200865	Male	White	25	12	Childhood onset. Persistent delusional thoughts, persecutory auditory hallucinations, impulsive and hyperactive behavior. Autistic brother. Psychosis scores at baseline (off meds): SAPS = 29, SANS = 49, BPRS24 = 87.
MH0217268	Female	White	49	-	-
MH0185900	Male	White	31	-	PANSS Total = 71

MH0185954	Female	Mixed (Non-Hispanic)	34	-	PANSS Total = 100
MH0185958	Female	White	56	-	PANSS Total = 88
MH0185963	Female	Black	47	-	PANSS Total = 71
MH0185970	Male	White	52	-	PANSS Total = 105
MH0185912	Male	White	34	-	PANSS Total = 106
MH0185945	Male	Hispanic	58	-	PANSS Total = 78
MH0185964	Female	Asian	43	-	PANSS Total = 72
MH0185966	Male	White	32	-	PANSS Total = 68
MH0185925	Male	Mixed (Null)	64	-	PANSS Total = 62
MH0185928	Female	Mixed (Non-Hispanic)	47	-	PANSS Total = 88

*All controls had no history or reported family history of Scz. Clinical psychometrics and age of onset provided only if known. No further information regarding mixed races was provided from the NIMH beyond the disclaimer that these individuals comprise more than one race. Mixed races were further categorized as “Hispanic” vs. “Non-Hispanic” or “Null” (missing or unknown).

Supplementary Table 2. NIMH iPSC donor sampling for major experiments.

Experiment & Figure	Sampling	Specific NIMH iPSC Donors
SOX2+ Progenitor Death (Figure 1c)	*n* = 20 iPSCs (5 Ctrl, 15 Scz)	**Ctrl:** MH0159019, MH0159021, MH0167170, MH0174677, MH0174686 **Scz:** MH0159025, MH0185223, MH0185225, MH0217268, MH0200865, MH0185900, MH0185912, MH0185925, MH0185928, MH0185945, MH0185954, MH0185958, MH0185964, MH0185966, MH0185970
Total MAP2+ Neurons (Figure 1d)	*n* = 21 iPSCs (4 Ctrl, 17 Scz)	**Ctrl:** MH0159019, MH0159020, MH0159021, MH0174677 **Scz:** MH0159025, MH0159026, MH0185223, MH0185225, MH0217268, MH0200865 MH0185900, MH0185912, MH0185925, MH0185928, MH0185945, MH0185954, MH0185958, MH0185963, MH0185964, MH0185966, MH0185970
Differentiation Pulse-Chase (Figure 1e)	*n* = 8 iPSCs (4 Ctrl, 4 Scz)	**Ctrl:** MH0159019, MH0159021, MH0167170, MH0174677 **Scz:** MH0159025, MH0185223, MH0185225, MH0200865
Single-Cell Sequencing (Figures 2-3)	*n* = 7 iPSCs (4 Ctrl, 3 Scz) *n* = 26,335 transcriptomes and *n* = 20,844 genes profiled in sum (group breakdowns provided in Legend for Figures 2-3)	**Ctrl:** MH0159019, MH0159020, MH0159021, MH0167170 **Scz:** MH0159025, MH0159026, MH0200865

BRN2-Virus BRN2+ Cells (Figure 4d)	*n* = 10 iPSCs (3 Ctrls, 5 Scz)	**Ctrl:** MH0159020, MH0159021, MH0174677 **Scz:** MH0159025, MH0159026, MH0185223, MH0185225, MH0200865
BRN2-Virus MAP2+ Cells (Figure 4e)	*n* = 10 iPSCs (5 Ctrls, 5 Scz)	**Ctrl:** MH0159019, MH0159020, MH0159021, MH0174677, MH0174686 **Scz:** MH0159025, MH0159026, MH0185223, MH0185225, MH0200865
BRN2-Virus Progenitor Death (Figure 4f)	*n* = 7 iPSCs (3 Ctrls, 4 Scz)	**Ctrl:** MH0159020, MH0159021, MH0174677 **Scz:** MH0159025, MH0185223, MH0185225, MH0200865
PTN Progenitor Death (Figure 5c)	*n* = 14 iPSCs (5 Ctrls, 9 Scz)	**Ctrl:** MH0159019, MH0159021, MH0167170, MH0174677, MH0174686 **Scz:** MH0159025, MH0185223, MH0185225, MH0217268, MH0200865, MH0185900, MH0185954, MH0185958, MH0185970
PTN Neurogenesis (Figure 5d)	*n* = 15 iPSCs (5 Ctrls, 10 Scz)	**Ctrl:** MH0159019, MH0159021, MH0167170, MH0174677, MH0174686 **Scz:** MH0159025, MH0185223, MH0185225, MH0217268, MH0200865, MH0185900, MH0185954, MH0185958, MH0185963, MH0185970

Supplementary Table 3. Top 10 most abundant proteins in organoids.

Protein Description	UniProt Accession	Gene Name	Control Intensity	Scz Intensity
Histone H4	H4_Human	HIST1H4A	3291771.845	2785097.087
Histone H2B	H2B1L_Human	HIST1H2BL	2592182.54	2265873.016
Histone H3.1	H31_Human	HIST1H3A	2222150.735	1894779.412
Actin, Cytoplasmic 2	ACTG_Human	ACTG1/ACTG	1404373.333	1417606.667
Histone H2A	A0A0U1RR32_Human	hCG_2039566	1286997.041	1089911.243
Histone H2A Type 2-B	H2A2B_Human	HIST2H2AB	1186519.231	1061596.154
Tubulin Alpha-1B chain	TBA1B_Human	TUBA1B	998203.991	724672.949
Thymosin beta-4	TYB4_Human	TMSB4X	703909.091	904840.909
Tubulin Beta-2A Chain	TBB2A_Human	TUBB2A/TUBB2	544202.247	356531.461
Peptidyl-prolyl Cis-Trans Isomerase A	PPIA_Human	PPIA/CYPA	426830.303	507715.152
Histone H1.5	H15_Human	HIST1H1B H1F5	391176.991	330516.593
Vimentin	VIME_Human	VIM	374522.532	458395.923

Supplementary Table 4. Neuronal and disease enrichment in organoids.

Pathway Database	Pathway Term	Protein Count	% of Proteome	*p* Value
Gene Ontology	GO:0043209: Myelin Sheath	120	3.3632287	3.34E-56
Gene Ontology	GO:0043025: Neuronal Cell Body	94	2.634529148	6.01E-06
Gene Ontology	GO:0030424: Axon	72	2.01793722	3.67E-06
Gene Ontology	Neurogenesis	69	1.933856502	6.07E-05
Gene Ontology	GO:0043005: Neuron Projection	68	1.905829596	4.42E-04
Gene Ontology	GO:0014069: Postsynaptic Density	50	1.401345291	0.008465825
Gene Ontology	Neuropathy	48	1.34529148	4.64E-14
Gene Ontology	GO:0007411: Axon Guidance	43	1.205156951	0.037049935
Gene Ontology	Epilepsy	36	1.00896861	0.002676137
Gene Ontology	GO:0031175: Neuron Projection Development	34	0.952914798	0.00195522
Gene Ontology	GO:0007409:Axonogenesis	28	0.784753363	0.052012199
Gene Ontology	GO:0010976: Positive Regulation of Neuron Projection Development	26	0.728699552	0.048697926
Gene Ontology	GO:0045773: Positive Regulation of Axon Extension	14	0.392376682	0.003550075

Gene Ontology	GO:1990090: Cellular Response to Nerve Growth Factor Stimulus	14	0.392376682	0.004992563
KEGG	HSA05016: Huntington's Disease	95	2.662556054	4.96E-11
KEGG	HSA05010: Alzheimer's Disease	84	2.35426009	3.89E-10
KEGG	HSA05012: Parkinson's Disease	76	2.130044843	4.97E-11
KEGG	HSA04530: Tight Junction	61	1.709641256	1.59E-05
KEGG	HSA04728: Dopaminergic Synapse	46	1.289237668	0.02644444
KEGG	HSA04520: Adherens Junction	35	0.980941704	1.36E-04
KEGG	HSA04721: Synaptic Vesicle Cycle	33	0.924887892	5.05E-05
KEGG	HSA04720: Long-Term Potentiation	25	0.700672646	0.06186726

Supplementary Table 5. Top 10 up-regulated proteins in Scz organoids.

Protein Description	UniProt Accession	Gene Name	FC Ratio (RSC)	*p* Value
MPV17	G5E9F5_Human	MPV17	156.26	2.84E-69
Neural Wiskott-Aldrich Syndrome Protein	WASL_Human	WASL	38.43	9.30E-78
Metallothionein-1X	MT1X_Human	MT1X	11.149	4.27E-21
Metallothionein-1H	MT1H_Human	MT1H	8.72	8.58E-18
Metallothionein-1F	MT1F_Human	MT1F	7.684	9.35E-16
Histone H1a (H1.1)	H11_Human	HIST1H1A	5.27	6.40E-11
Lithostathine-1-Alpha	REG1A_Human	REG1A	4.842	4.69E-10
Uncharacterized Protein	MOR296_Human	-	4.739	7.58E-10
Tropomyosin Beta Chain	TPM2_Human	TPM2	4.156	1.68E-08
Olfactomedin-4	OLM4_Human	OLM4	4.149	1.65E-08

Supplementary Table 6. Top 10 down-regulated proteins in Scz organoids.

Protein Description	UniProt Accession	Gene Name	FC Ratio (RSC)	*p* Value
Myosin-4	MYH4_Human	MYH4	-5.654	2.65E-14
Phosphoinositide Phospholipase C-Like 1	H3BUD4_Human	PLCL1	-4.977	7.04E-13
Myosin-13	MYH13_Human	MYH13	-4.363	3.19E-11
Troponin C	TNNC1_Human	TNNC1	-4.195	7.47E-11
Myosin-3	MYH3_Human	MYH3	-4.111	1.41E-10
Troponin C 2	TNNC2_Human	TNNC2	-3.917	5.99E-10
Histone H2B	U3KQK0_Human	HIST1H2BN	-3.866	9.02E-10
Insulin	A6XGL2_Human	INS	-3.845	9.63E-10
Myosin Regulatory Light Chain 2	MLRS_Human	MYLPF	-3.665	2.39E-09
Myosin Light Chain 1/3	MYL1_Human	MYL1	-2.834	8.93E-07

Supplementary Table 7. Top up-regulated GO pathways (proteomics).

Pathway Term	Fold Enrichment	*p* Value	Bonferroni Value	False Discovery Rate
Extracellular Exosome	3.65317658	1.08E-25	2.50E-23	1.39E-22
Acetylation	2.79242172	1.17E-14	2.60E-12	1.49E-11
Extracellular Space	3.328643311	5.98E-09	1.39E-06	7.68E-06
Annexin*	69.45219348	1.52E-08	3.39E-06	1.94E-05
Calcium/Phospholipid Binding	64.82204724	2.27E-08	5.06E-06	2.90E-05
Disease Mutation	2.542041068	3.01E-08	6.70E-06	3.83E-05
Cadherin Binding Involved in Cell-Cell Adhesion	6.73508122	1.47E-07	3.77E-05	1.92E-04
Brush Border	19.28465608	1.72E-07	4.00E-05	2.21E-04
Phosphoprotein	1.572205851	2.27E-07	5.06E-05	2.90E-04
Collagen Fibril Organization	24.30603805	3.66E-07	3.47E-04	5.74E-04

*****Due to repeat protein classifications, Annexin-related pathway categories (namely, IPR001464: Annexin, IPR018252: Annexin Repeat Conserved Site, IPR018502: Annexin Repeat, Repeat: Annexin 1, Repeat: Annexin 3, Repeat: Annexin 4, Repeat: Annexin 2, & SM00335: ANX) were the 5^{th}-12^{th} and 14^{th} most significant up-regulated enrichment terms. These categories have been omitted here for repetition, brevity and diversity. Categories ranked by significance.

Supplementary Table 8. Top down-regulated GO pathways (proteomics).

Pathway Term	Fold Enrichment	*p* Value	Bonferroni Value	False Discovery Rate
Muscle Protein*	126.7451613	3.65E-38	4.70E-36	4.24E-35
Muscle Filament Sliding*	150.0774578	3.23E-34	1.12E-31	4.41E-31
Muscle Myosin Complex*	189.8333333	3.71E-17	3.97E-15	4.17E-14
Troponin Complex*	253.1111111	9.54E-12	1.02E-09	1.07E-08
Cardiac Muscle Contraction*	56.32536688	7.44E-11	2.58E-08	1.02E-07
Actin Binding*	15.02262774	2.12E-09	2.74E-07	2.47E-06
Domain: IQ	36.54462659	5.64E-07	4.45E-04	8.64E-04
Disease Mutation	3.228392157	7.20E-07	9.29E-05	8.37E-04
Methylation	5.233566434	1.36E-06	1.76E-04	0.001582906
Calmodulin Binding	17.23289474	2.83E-06	3.65E-04	0.003295404

*****Due to repeat protein classifications, largely derived from pathways with overlap involving myosin-, troponin- and actin-related proteins, several GO categories with higher significance than Domain:IQ, Disease Mutation, Methylation and Calmodulin Binding were omitted. These included protein classifications consisting of GO:0003009: Skeletal Muscle Contraction, Thick Filament, GO:0032982: Myosin Filament, GO:0006936: Muscle Contraction, Myosin, GO:0008307: Structural Constituent of Muscle, IPR004009: Myosin N-Terminal SH3-Like, GO:0030017: Sarcomere, IPR002928: Myosin Tail, IPR027401: Myosin-Like IQ Motif, Motor Proteins, GO:0000146: Microfilament Motor Activity, GO:0003779: Actin Binding, Region of Interest: Actin Binding, Domain: Myosin Head-Like, GO:0006937: Regulation of Muscle Contraction, IPR001609: Myosin Head, Motor Domain, SM00242: MYSc, IPR001978: Troponin, GO:0114883: Transition Between Fast and Slow, GO:0030017: Z Disc, GO:0030016: Myofibril, & GO:0051015: Actin Filament Binding. These GO categories largely reflect the early classification of myosins and other related proteins to muscle pathways and protein classification sets, despite being found in other organs, tissues and cell groups of non-muscular origin. Categories ranked by significance.

SUPPLEMENTARY REFERENCES

1. Camp, J.G., F. Badsha, M. Florio, S. Kanton, T. Gerber, M. Wilsch-Bräuninger, et al., *Human cerebral organoids recapitulate gene expression programs of fetal neocortex development.* Proc Nat Acad Sci, 2015. **112**(51): p. 15672-15677.
2. Lancaster, M.A., M. Renner, C.-A. Martin, D. Wenzel, L.S. Bicknell, M.E. Hurles, et al., *Cerebral organoids model human brain development and microcephaly.* Nature, 2013. **501**(7467): p. 373.
3. Luo, C., M.A. Lancaster, R. Castanon, J.R. Nery, J.A. Knoblich, & J.R. Ecker, *Cerebral organoids recapitulate epigenomic signatures of the human fetal brain.* Cell Reports, 2016. **17**(12): p. 3369-3384.
4. Sharma, A., K. Singh, & A. Almasan, *Histone H2AX phosphorylation: a marker for DNA damage*, in *DNA Repair Protocols*. 2012, Springer. p. 613-626.
5. Kuo, L.J. & L.-X. Yang, *γ-H2AX-a novel biomarker for DNA double-strand breaks.* In Vivo, 2008. **22**(3): p. 305-309.
6. Ha, L., S. Ceryak, & S.R. Patierno, *Generation of S phase-dependent DNA double-strand breaks by Cr (VI) exposure: involvement of ATM in Cr (VI) induction of γ-H2AX.* Carcinogenesis, 2004. **25**(11): p. 2265-2274.
7. Paull, T.T., E.P. Rogakou, V. Yamazaki, C.U. Kirchgessner, M. Gellert, & W.M. Bonner, *A critical role for histone H2AX in recruitment of repair factors to nuclear foci after DNA damage.* Current Biol, 2000. **10**(15): p. 886-895.
8. Iwamoto, K., M. Bundo, & T. Kato, *Altered expression of mitochondria-related genes in postmortem brains of patients with bipolar disorder or schizophrenia, as revealed by large-scale DNA microarray analysis.* Hum Mol Genet, 2004. **14**(2): p. 241-253.
9. Torrell, H., Y. Alonso, G. Garrabou, D. Mulet, M. Catalán, A. Valiente-Pallejà, et al., *Mitochondrial dysfunction in a family with psychosis and chronic fatigue syndrome.* Mitochondrion, 2017. **34**: p. 1-8.
10. Wegner, A.M., C.A. Nebhan, L. Hu, D. Majumdar, K.M. Meier, A.M. Weaver, et al., *N-wasp and the arp2/3 complex are critical regulators of actin in the development of dendritic spines and synapses.* J Biol Chem, 2008. **283**(23): p. 15912-15920.
11. Glantz, L.A. & D.A. Lewis, *Decreased dendritic spine density on prefrontal cortical pyramidal neurons in schizophrenia.* Arch Gen Psychiatry, 2000. **57**(1): p. 65-73.
12. Kolluri, N., Z. Sun, A.R. Sampson, & D.A. Lewis, *Lamina-specific reductions in dendritic spine density in the prefrontal cortex of subjects with schizophrenia.* Am J Psychiatry, 2005. **162**(6): p. 1200-1202.
13. Datta, D., D. Arion, K.M. Roman, D.W. Volk, & D.A. Lewis, *Altered expression of ARP2/3 complex signaling pathway genes in prefrontal layer 3 pyramidal cells in schizophrenia.* Am J Psychiatry, 2016. **174**(2): p. 163-171.
14. Colantuoni, C., B.K. Lipska, T. Ye, T.M. Hyde, R. Tao, J.T. Leek, et al., *Temporal dynamics and genetic control of transcription in the human prefrontal cortex.* Nature, 2011. **478**(7370): p. 519-523.
15. Wu, Y., Y.-G. Yao, & X.-J. Luo, *SZDB: a database for schizophrenia genetic research.* Schizophr Bull, 2017. **43**(2): p. 459-471.

16. Wu, Y., X. Li, J. Liu, X.J. Luo, & Y.G. Yao, *SZDB2. 0: an updated comprehensive resource for schizophrenia research.* Hum Genet, 2020.
17. Jia, P., G. Han, J. Zhao, P. Lu, & Z. Zhao, *SZGR 2.0: a one-stop shop of schizophrenia candidate genes.* Nucleic Acids Res, 2017. **45**(D1): p. D915-D924.
18. Pardiñas, A.F., P. Holmans, A.J. Pocklington, V. Escott-Price, S. Ripke, N. Carrera, et al., *Common schizophrenia alleles are enriched in mutation-intolerant genes and in regions under strong background selection.* Nat Genet, 2018. **50**(3): p. 381-389.
19. Ripke, S., B.M. Neale, A. Corvin, J.T. Walters, K.-H. Farh, P.A. Holmans, et al., *Biological insights from 108 schizophrenia-associated genetic loci.* Nature, 2014. **511**(7510): p. 421-427.
20. Jaffe, A.E., Y. Gao, A. Deep-Soboslay, R. Tao, T.M. Hyde, D.R. Weinberger, et al., *Mapping DNA methylation across development, genotype and schizophrenia in the human frontal cortex.* Nat Neurosci, 2016. **19**(1): p. 40-47.
21. Kinoshita, M., S. Numata, A. Tajima, K. Ohi, R. Hashimoto, S. Shimodera, et al., *Aberrant DNA methylation of blood in schizophrenia by adjusting for estimated cellular proportions.* Neuromol Med, 2014. **16**(4): p. 697-703.
22. Wockner, L.F., E.P. Noble, B.R. Lawford, R.M. Young, C.P. Morris, V.L. Whitehall, et al., *Genome-wide DNA methylation analysis of human brain tissue from schizophrenia patients.* Transl Psychiatry, 2014. **4**(1): p. e339-e339.